Inorg. Chem. **2005**, *44*, 3551–3560

Complexes of Functionalized Dipyrido[3,2-*a*:2′,3′-*c*]-phenazine: A Synthetic, Spectroscopic, Structural, and Density Functional Theory Study

Natasha J. Lundin,[†] Penny J. Walsh,[†] Sarah L. Howell,[†] John J. McGarvey,[‡] Allan G. Blackman,*[,†] and Keith C. Gordon*[,†]

Department of Chemistry, MacDiarmid Institute for Advanced Materials and Nanotechnology, University of Otago, Union Place, P.O. Box 56, Dunedin, New Zealand, and School of Chemistry, Queen's University Belfast, Belfast BT9 5AG, Northern Ireland

Received February 2, 2005

The ligands 11-bromodipyrido[3,2-*a*:2′,3′-*c*]phenazine and ethyl dipyrido[3,2-*a*:2′,3′-*c*]phenazine-11-carboxylate have been prepared and coordinated to ruthenium(II), rhenium(I), and copper(I) metal centers. The electronic effects of substitution of dipyrido[2,3-*a*:3′,2′-*c*]phenazine (dppz) have been investigated by spectroscopy and electrochemistry, and some photophysical properties have been studied. The crystal structures of $[Re(L)(CO)_3Cl]$ (L = ethyl dipyrido-[3,2-*a*:2′,3′-*c*]phenazine-11-carboxylate or 11-bromodipyrido[3,2-*a*:2′,3′-*c*]phenazine) are presented. Density functional theory calculations on the complexes show only small deviations in bond lengths and angles (most bonds within 0.02 Å, most angles within 2°) from the crystallographic data. Furthermore, the vibrational spectra of the strongest Raman and IR bands are predicted to within an average 6 cm^{-1} for the complexes $[Re(L)(CO)_3Cl]$ and $[Cu(L)(triphenylphosphine)_2]BF_4$ (in the 1000–1700 cm^{-1} region). Spectroscopic and electrochemical evidence suggest that reduction of the complex causes structural changes across the entire dppz ligand. This is unusual as dppz-based ligands typically have electrochemical properties that suggest charge localization with reduction on the phenazine portion of the ligand. The excited-state lifetimes of the complexes have been measured, and they range from ca. 200 ns for the $[Ru(L)(2,2′\text{-bipyridine})_2](PF_6)_2$ complexes to over 2 μs for [Cu(11-bromodipyrido[3,2-*a*:2′,3′-*c*]phenazine)$(PPh_3)_2$](BF_4) at room temperature. The emission spectra suggest that the unusually long-lived excited states of the copper complexes result from metal-to-ligand charge transfer (MLCT) transitions as they are completely quenched in methanol. Electroluminescent films may be fabricated from these compounds; they show MLCT state emission even at low doping levels [<0.1% by weight in poly(vinylcarbazole) polymer matrix].

Introduction

Dipyrido[3,2-*a*:2′,3′-*c*]phenazine (dppz) (Figure 1) is a heterocyclic aromatic ligand whose complexes have received much attention in recent years, primarily because the planarity and extended aromatic nature of dppz gives it the ability to intercalate with DNA.[1−9] Ruthenium-based polypyridyl complexes containing dppz[3] have been of specific interest because of their intense fluorescence upon association with DNA. Complexes of this type have been tagged "molecular light switches" because, although the fluorescence of these complexes in aqueous solutions is negligible, increases of greater than 10 000-fold in the presence of DNA

* Authors to whom correspondence should be addressed. Fax: +64-3-479-7906. E-mail: kgordon@alkali.otago.ac.nz (K.C.G.); blackman@alkali.otago.ac.nz (A.G.B.).

[†] University of Otago.

[‡] Queen's University Belfast.

(1) Stoeffler, H. D.; Thornton, N. B.; Temkin, S. L.; Schanze, K. S. *J. Am. Chem. Soc.* **1995**, *117*, 7119.
(2) Hiort, C.; Lincoln, P.; Norden, B. *J. Am. Chem. Soc.* **1993**, *115*, 3448.
(3) Turro, C.; Bossmann, S. H.; Jenkins, Y.; Barton, J. K.; Turro, N. J. *J. Am. Chem. Soc.* **1995**, *117*, 9026.
(4) Yam, V. W.-W. V.; Lo, K. K.-W.; Cheung, K.-K.; Kong, R. Y.-C. *J. Chem. Soc., Dalton Trans.* **1997**, 2067.
(5) Friedman, A. E.; Chambron, J. C.; Sauvage, J. P.; Turro, N. J.; Barton, J. K. *J. Am. Chem. Soc.* **1990**, *112*, 4960.
(6) Coates, C. G.; McGarvey, J. J.; Callaghan, P. L.; Coletti, M.; Hamilton, J. G. *J. Phys. Chem. B* **2001**, *105*, 730.
(7) Coates, C. G.; Callaghan, P.; McGarvey, J. J.; Kelly, J. M.; Jacquet, L.; Kirsch-De Mesmaeker, A. *J. Mol. Struct.* **2001**, *598*, 15.
(8) Coates, C. G.; Olofsson, J.; Coletti, M.; McGarvey, J. J.; Oenfelt, B.; Lincoln, P.; Norden, B.; Tuite, E.; Matousek, P.; Parker, A. W. *J. Phys. Chem. B* **2001**, *105*, 12653.
(9) Coates, C. G.; Callaghan, P. L.; McGarvey, J. J.; Kelly, J. M.; Kruger, P. E.; Higgins, M. E. *J. Raman Spectrosc.* **2000**, *31*, 283.

10.1021/ic050179k CCC: $30.25
Published on Web 04/21/2005

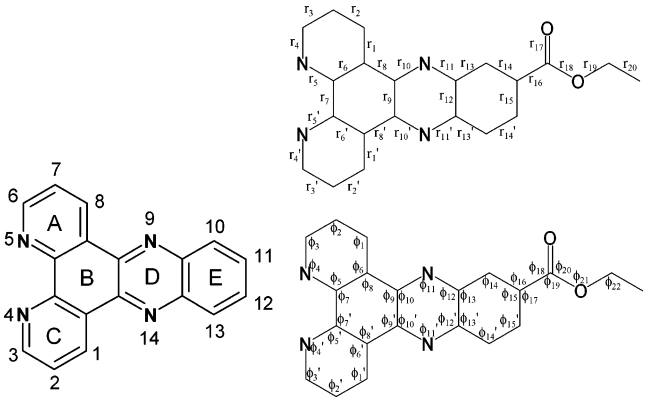

Figure 1. Structure of dppz, showing ring labels and IUPAC numbering (left) and the bond and angle labeling of the cis rotamer of **1** (right).

have been observed.[4] Complexes of dppz derivatives are also useful as components in organic light-emitting devices (OLEDs) because their emission color is largely red-shifted from their absorption wavelength.[10,11]

Dppz is also interesting from the perspective of its electronic structure. The properties of dppz suggest that reduction of the ligand, or complexes containing these ligands, leads to the formation of a radical anion with a charge located on the phenazine portion of the ligand.[12−16] This may be interpreted in terms of the presence of unoccupied molecular orbitals (MOs), which are localized over either the phenanthroline (phen; rings A, B, C) or the phenazine (phz; rings B, D, E) regions of the ligand.[17] This MO model, which has been used to rationalize the properties of dppz complexes, was developed in a series of papers by Kaim et al.[12−16] The excited-state electronic properties of the dppz complexes are also interesting because the metal-to-ligand charge transfer (MLCT) excited states can be similar in energy to ligand-centered (LC) states.[17] Through judicious selection of the metal ion coordinated to dppz, one can tune the nature of the lowest-energy excited state from MLCT to LC.[18] The low orbital overlap between the dπ and ligand π* MOs results in such complexes being virtually colorless (in the absence of other chromophoric ligands) as the MLCT transition is raised in energy from the visible to the ultraviolet region and lowered in intensity.[11]

It is possible to tune the energy level of the phz-based lowest unoccupied MO (LUMO) by substitution of the aromatic skeleton of dppz. Electron-withdrawing groups result in less-negative reduction potentials, and an electron-donating group at the same position is expected to have the opposite effect.[18] One way to probe these substituent effects is to model the complexes of interest using computational methods such as density functional theory (DFT).

Computational chemistry allows the possibility of modeling metal polypyridyl systems, providing structural and energetic information. One of the early examples in this field was a study by Broo and Lincoln.[19] They used semiempirical intermediate neglect of differential overlap methods to model a number of ruthenium(II) polypyridyl complexes, including dppz complexes. These calculations were compared with the ab initio Hartree−Fock (HF) method, with the ruthenium(II) center approximated by the effective core potential of Stevens et al.,[20] which includes 28 core electrons and the valence double-ζ basis set. Basis sets for the other atoms were the minimal STO-3G or the 6-31G basis set. The STO-3G basis set calculations are the least accurate because this is the smallest basis set one can use in HF methods. The 6-31G basis set is also limited because it does not contain any polarization functions, which have been found to be very important in systems containing larger atoms.[21] The HF method has the fundamental shortcoming of not including electron correlation appropriately, which is important in extended π systems. DFT offers a method that includes correlation and is generally more accurate than HF methods.[22]

DFT has been used to study metal polypyridyl complexes.[23−25] Dattelbaum et al.[23] used DFT/B3LYP calculations to model the geometries and associated energies of $[Re(CO)_3(4,4'\text{-}X_2bpy)(4\text{-ethylpyridine})]^+$ complexes (X = CH_3, H, COOEt) and to identify mixing of π*(4,4′-X_2bpy) and π*(CO) MOs. They described the rhenium(I) center using the LANL2 effective core potential and associated basis set and other atoms using the 6-31G(d) basis set. In another study, Dattelbaum et al.[24] used the DFT/B3LYP theory to determine geometries and vibrational frequencies of both the ground singlet state and the lowest triplet state of *fac*-$[Re(CO)_3(pp)(L)]^+$ complexes [pp = polypyridyl ligand L = 4-ethylpyridine, 1-methyl-6-oxyquinone, or 10-(4-picolyl)-phenothiazine]. They used the "small core" LANL2 relativistic effective core potential and associated basis set to describe the rhenium(I) center[26] and the 6-31G(d) basis set for the ligands. Time-dependent DFT calculations were used to calculate the energies of excited states from the ground-state geometry. Calculated vibrational frequencies of excited states were compared with time-resolved infrared measurements. Changes in the carbonyl absorptions upon excitation

(10) David, G.; Walsh, P. J.; Gordon, K. C. *Chem. Phys. Lett.* **2004**, *383*, 292.
(11) Gordon, K. C.; Walsh, P. J.; McGale, E. M. *Curr. Appl. Phys.* **2004**, *4*, 331.
(12) Baumann, F.; Kaim, W.; Posse, M. G.; Katz, N. E. *Inorg. Chem.* **1998**, *37*, 658.
(13) Fees, J.; Kaim, W.; Moscherosch, M.; Matheis, W.; Klima, J.; Krejcik, M.; Zalis, S. *Inorg. Chem.* **1993**, *32*, 166.
(14) Fees, J.; Ketterle, M.; Klein, A.; Fiedler, J.; Kaim, W. *J. Chem. Soc., Dalton Trans.* **1999**, 2595.
(15) Klein, A.; Kaim, W.; Waldhoer, E.; Hausen, H.-D. *J. Chem. Soc., Perkin Trans. 2* **1995**, 2121.
(16) Klein, A.; Scheiring, T.; Kaim, W. *Z. Anorg. Allg. Chem.* **1999**, *625*, 1177.
(17) Waterland, M. R.; Gordon, K. C. *J. Raman Spectrosc.* **2000**, *31*, 243.
(18) Waterland, M. R.; Gordon, K. C.; McGarvey, J. J.; Jayaweera, P. M. *J. Chem. Soc., Dalton Trans.* **1998**, 609.
(19) Broo, A.; Lincoln, P. *Inorg. Chem.* **1997**, *36*, 2544.
(20) Stevens, W. J.; Basch, H.; Krauss, M. *J. Chem. Phys.* **1984**, *81*, 6026.
(21) Foresman, J. B.; Frisch, A. *Exploring Chemistry with Electronic Strucuture Methods*, 2nd ed.; Gaussian, Inc.: Pittsburgh, 1995.
(22) Young, D. C. *Computational Chemistry: A Practical Guide for Applying Techniques to Real-World Problems*; Wiley: New York, 2001.
(23) Dattelbaum, D. M.; Martin, R. L.; Schoonover, J. R.; Meyer, T. J. *J. Phys. Chem. A* **2004**, *108*, 3518.
(24) Dattelbaum, D. M.; Omberg, K. M.; Hay, P. J.; Gebhart, N. L.; Martin, R. L.; Schoonover, J. R.; Meyer, T. J. *J. Phys. Chem. A* **2004**, *108*, 3527.
(25) Wilhelmsson, L. M.; Esbjoerner, E. K.; Westerlund, F.; Norden, B.; Lincoln, P. *J. Phys. Chem. B* **2003**, *107*, 11784.
(26) Russo, T. V.; Martin, R. L.; Hay, P. J. *J. Phys. Chem.* **1995**, *99*, 17085.

were monitored and compared with characteristic patterns in the carbonyl absorptions of transient states. This method was used to assign excited states.

This study investigates the structural and electronic effects of substituting dppz at the 11 position with a bromide or an ethyl ester group and, subsequently, the effect of coordination of a metal center to the substituted ligands. The synthesis of these ligands and their $[Re(L)(CO)_3Cl]$, $[Ru(L)(bpy)_2](PF_6)_2$, and $[Cu(L)(PPh_3)_2]BF_4$ (bpy = 2,2′-bipyridine, PPh_3 = triphenylphosphine) complexes is reported. The crystal structures $[Re(L)(CO)_3Cl]$ (where L = ethyl dipyrido[3,2-*a*:2′,3′-*c*]phenazine-11-carboxylate or 11-bromodipyrido[3,2-*a*:2′,3′-*c*]phenazine) are presented and compared with structures obtained from DFT calculations. The electronic properties of the ligands and their complexes are investigated using UV−vis absorption spectroscopy and cyclic voltammetry, and excited-state properties are explored using fluorimetry and lifetime measurements.

Experimental Section

Materials. Commercially available reagents were used as received. Literature procedures were used to prepare the precursor 1,10-phenanthroline-5,6-dione,[27] 4-bromo-1,2-benzenediamine,[28,29] *cis*-$[Ru(bpy)_2Cl_2]$,[30] and $[Cu(PPh_3)_4]BF_4 \cdot H_2O$.[31] Ligands were prepared by the Schiff-base condensation of 1,10-phenanthroline-5,6-dione with the appropriate diamino compound. All metal complexes were synthesized by established literature techniques with minor variations.[18,31,32] Spectroscopic grade solvents were dried and filtered through neutral aluminum oxide before being used for electrochemical and spectroscopic measurements.

Instrumentation. Electronic spectra were recorded on a Varian Cary 500 Scan UV−vis−NIR spectrophotometer. Emission spectra were recorded on a Perkin-Elmer luminescence spectrometer LS 50 B. ^{1}H NMR spectra were recorded on a Varian Unity Inova-300 2-Channel FT 300 MHz spectrometer at 25 °C. Chemical shifts are reported relative to residual solvent signals. Elemental analyses were performed by the Campbell Microanalytical Laboratory, University of Otago. FT-IR spectra were recorded in the solid state (KBr disk) on a Perkin-Elmer Spectrum BX FT-IR System with Spectrum v. 2.00. Melting points were recorded on a Kofler Heizbank hot-stage apparatus. Cyclic voltammograms were recorded from nitrogen-purged 0.5 mM dichloromethane or acetonitrile solutions with 0.1 M tetrabutylammonium perchlorate as the supporting electrolyte. The electrochemical cell consisted of a 1-mm-diameter platinum working electrode embedded in a KeL-F cylinder with a platinum auxiliary electrode and a saturated potassium chloride calomel reference electrode. The cyclic voltammograms were calibrated against the decamethylferrocene/decamethylferrocenium couple. The potential of the cell was controlled by an EG&G PAR 273A potentiostat with model 270 software. Emission lifetime measurements were made using a nanosecond-pulsed excitation source (Spectra-Physics Quanta-Ray, Model DCR Nd^{3+}:YAG laser). Emission signals at various detection wavelengths were measured with a photomultiplier tube (Model RCA 1P28) in which several of the dynodes were wired to the anode as in the circuit described by Hunt and Thomas[33] to provide a rapid response. Kinetic traces were recorded using a digital oscilloscope (Tektronix model TDS 3032). All measurements were of approximately 4×10^{-5} M solutions made up in spectrophotometric grade solvents at room temperature. Solutions were purged with argon for 10 min prior to measurement. UV−vis spectra were collected before and after emission lifetime measurements in order to check that no sample degradation had occurred. Incident pulse energies were typically ~10 mJ. The emission lifetime was determined by fitting a single-exponential function to each signal. Emission signals were collected at 2−3 wavelengths for each sample, and the reported lifetimes are the mean of these measurements. FT-Raman spectra were collected on powder samples using a Bruker IFS-55 interferometer with an FRA/106S attachment. The excitation source was a Nd:YAG laser with an excitation wavelength of 1064 nm. An InGaAs diode (D424) operating at room temperature was used to detect Raman photons. All spectra were taken with a laser power of 105 mW at the sample and a resolution of 4 cm^{-1}, using 16−64 scans.

Ethyl 3,4-Diaminobenzoate. 3,4-diaminobenzoic acid (500 mg, 3.3 mmol) was suspended in ethanol (30 mL). Concentrated H_2SO_4 (1 mL) was added dropwise, and the mixture was refluxed for 6 h. The solution was concentrated, and then H_2O (30 mL) was added. Aqueous NaOH (1 M) was added until the pH was 10, and the product was extracted into $CHCl_3$. The organic layer was washed with H_2O, dried with $MgSO_4$, and evaporated to give a light brown powder (480 mg, 81%). ^{1}H NMR ($CDCl_3$): δ_H 1.36 (t, 3H, J = 6.9 Hz), 3.40 (bs, 4H), 4.31 (q, 2H, J = 6.9 Hz), 6.67 (d, 1H, J = 8.1 Hz), 7.41 (s, 1H), 7.49 (d, 1H, J = 8.1 Hz) ppm. Anal. Calcd for $C_9H_{12}N_2O_2$: C, 59.98; H, 6.71; N, 15.55. Found: C, 59.84; H, 6.61; N, 15.24.

Ethyl Dipyrido[3,2-*a*:2′,3′-*c*]phenazine-11-carboxylate·0.5H_2O (1). 1,10-phenanthroline-5,6-dione (585 mg, 2.8 mmol) and ethyl 3,4-diaminobenzoate (500 mg, 2.8 mmol) were suspended in ethanol (80 mL), and the suspension was refluxed for 1 h. The solvent was removed, the resulting solid was dissolved in $CHCl_3$, and the solution was filtered through Celite. The filtrate was purified by column chromatography on neutral alumina ($CHCl_3$), yielding the product as a light brown powder (421 mg, 43%). ^{1}H NMR ($CDCl_3$): δ_H 1.52 (t, 3H, J = 7.2 Hz), 4.54 (q, 2H, J = 7.2 Hz), 7.81 (q, 2H, J = 4.5 Hz), 8.38 (d, 1H, J = 8.7 Hz), 8.50 (dd, 1H, J = 2.1, 8.7 Hz), 9.07 (d, 1H, J = 1.5 Hz), 9.29 (t, 2H, J = 2.7 Hz), 9.63 (d, 2H, J = 8.1 Hz) ppm. Anal. Calcd for $C_{21}H_{15}N_4O_{2.5}$: C, 69.41; H, 4.16; N, 15.42. Found: C, 69.72; H, 4.17; N, 15.19.

11-Bromodipyrido[3,2-*a*:2′,3′-*c*]phenazine (2). 2 was prepared in the same manner as **1**, except that 4-bromo-1,2-benzenediamine was used instead of ethyl 3,4-diaminobenzoate. The product was obtained as a light brown solid (757 mg, 75%). ^{1}H NMR ($CDCl_3$): δ_H 7.77 (q, 2H, J = 4.5, 7.8 Hz), 7.95 (dd, 1H, J = 2.1, 9 Hz), 8.16 (d, 1H, J = 9 Hz), 8.49 (d, 1H, J = 2.4 Hz), 9.26 (dd, 2H, J = 1.8, 4.5 Hz), 9.52 (m, 2H) ppm. Anal. Calcd for $C_{18}H_9N_4Br$: C, 59.85; H, 2.51; N, 15.52; Br, 22.12. Found: C, 60.01; H, 2.75; N, 15.25; Br, 22.05.

[$Cu(PPh_3)_2$(ethyl dipyrido[3,2-*a*:2′,3′-*c*]phenazine-11-carboxylate)]$BF_4 \cdot H_2O$ (3). Diethyl ether (30 mL) was purged with N_2 for 15 min, then $[Cu(PPh_3)_4]BF_4$ (338 mg, 0.28 mmol) and **1** (100 mg, 0.28 mmol) were added, and the suspension was stirred for 55 h under N_2 at room temperature. The resulting yellow

(27) Smith, G. F.; Cagle, F. W., Jr. *J. Org. Chem.* **1947**, *12*, 781.
(28) Elder, J. W. *J. Chem. Educ.* **1994**, *71*, A142.
(29) Wilson, J. G.; Hunt, F. C. *Aust. J. Chem.* **1983**, *36*, 2317.
(30) Marmion, M. E.; Takeuchi, K. J. *J. Am. Chem. Soc.* **1988**, *110*, 1472.
(31) Rader, R. A.; McMillin, D. R.; Buckner, M. T.; Matthews, T. G.; Casadonte, D. J.; Lengel, R. K.; Whittaker, S. B.; Darmon, L. M.; Lytle, F. E. *J. Am. Chem. Soc.* **1981**, *103*, 5906.
(32) Browne, W. R.; O'Connor, C. M.; Hughes, H. P.; Hage, R.; Walter, O.; Doering, M.; Gallagher, J. F.; Vos, J. G. *J. Chem. Soc., Dalton Trans.* **2002**, 4048.
(33) Hunt, J. W.; Thomas, J. K. *Radiat. Res.* **1967**, *32*, 149.

precipitate was isolated by filtration and recrystallized from methanol to give a bright yellow powder (157 mg, 54%). Anal. Calcd for $C_{57}H_{46}N_4BO_3F_4P_2Cu$: C, 65.37; H, 4.43; N, 5.35; P, 5.91. Found: C, 65.24; H, 4.25; N, 5.35; P, 6.08.

[Cu(PPh$_3$)$_2$(11-bromodipyrido[3,2-*a*:2′,3′-*c*]phenazine)]BF$_4$ (4). This complex was prepared in the same manner as **3** but using ligand **2** instead of **1**, yielding a bright yellow powder (226 mg, 78%). Anal. Calcd for $C_{54}H_{39}N_4BF_4P_2CuBr$: C, 62.60; H, 3.79; N, 5.41; P, 5.98; Br, 7.71. Found: C, 62.30; H, 3.87; N, 5.37; P, 5.78; Br, 7.54.

[Ru(bpy)$_2$(ethyl dipyrido[3,2-*a*:2′,3′-*c*]phenazine-11-carboxylate)](PF$_6$)$_2$ (5). *cis*-[Ru(bpy)$_2$Cl$_2$] (104 mg, 0.2 mmol) and **1** (100 mg, 0.28 mmol) were dissolved in ethanol/H_2O (1:1, 10 mL), and the solution was refluxed overnight. The solvent was removed on the rotary evaporator, the residue was dissolved in water (20 mL), and the solution was filtered to remove unreacted ligand. Saturated aqueous $NaPF_6$ (2 mL) was added dropwise to the stirred filtrate, and the resulting orange precipitate was isolated by filtration; washed with water (2 × 10 mL), methanol (1 × 10 mL), and ether (1 × 10 mL); and air-dried. The red-brown solid was suspended in boiling methanol (20 mL) for 1 h, resulting in a bright orange powder, which was isolated by filtration to give **5** (203 mg, 94%). ^{1}H NMR ($CDCl_3$): δ_H 1.52 (t, 3H, J = 7.5 Hz), 4.54 (q, 2H, J = 7.2, 14.4 Hz), 7.83 (dd, 2H, J = 4.5, 8.1 Hz), 8.42 (d, 1H, J = 8.7 Hz), 8.52 (dd, 1H, J = 1.2, 9 Hz), 9.10 (d, 1H, J = 2.1 Hz), 9.31 (dd, 2H, J = 2.4, 3.6 Hz), 9.68 (dd, 2H, J = 0.9, 9 Hz) ppm. Anal. Calcd for $C_{41}H_{30}N_8O_2F_{12}P_2Ru$: C, 46.55; H, 2.86; N, 10.60; P, 5.76. Found: C, 46.77; H, 2.90; N, 10.76; P, 5.57.

[Ru(bpy)$_2$(11-bromodipyrido[3,2-*a*:2′,3′-*c*]phenazine)](PF$_6$)$_2$.H$_2$O (6). This complex was prepared in the same manner as **5** but using ligand **2** instead of **1**, giving the product as an orange powder (193 mg, 89%). Anal. Calcd for $C_{38}H_{27}N_8OF_{12}P_2BrRu$: C, 42.16; H, 2.51; N, 10.35; Br, 7.38. Found: C, 42.23; H, 2.46; N, 10.20; Br, 7.52.

[Re(CO)$_3$Cl(ethyl dipyrido[3,2-*a*:2′,3′-*c*]phenazine-11-carboxylate)] (7). Ethanol (40 mL) was degassed with N_2 for 15 min; then, [Re(CO)$_5$Cl] (50 mg, 0.14 mmol) and **1** (49 mg, 0.14 mmol) were added, and the solution was refluxed for 5 h. The solution was cooled on ice, and the resulting orange precipitate was filtered (74 mg, 81%). Crystals suitable for X-ray diffraction were grown by slow evaporation of a dichloromethane solution. ^{1}H NMR ($CDCl_3$): δ_H 1.54 (t, 3H, J = 6.9 Hz), 4.56 (q, 2H, J = 6.6 Hz), 8.03 (t, 2H, J = 5.7 Hz), 8.39 (d, 1H, J = 8.7 Hz), 8.58 (d, 1H, J = 8.7 Hz), 9.06 (s, 1H), 9.46 (d, 2H, J = 3.6 Hz), 9.77 (d, 2H, J = 7.8 Hz) ppm. Anal. Calcd for $C_{24}H_{14}N_4O_5ClRe$: C, 43.67; H, 2.14; N, 8.49; Cl, 5.37. Found: C, 43.91; H, 2.02; N, 8.58; Cl, 5.33.

[Re(CO)$_3$Cl(11-bromodipyrido[3,2-*a*:2′,3′-*c*]phenazine)] (8). The complex was synthesized in the same manner as **7** but using ligand **2** instead of **1**. The desired product was obtained as a yellow powder (64 mg, 69%). Crystals suitable for X-ray diffraction were grown by slow evaporation of a dichloromethane solution. ^{1}H NMR ($CDCl_3$): δ_H 8.03 (s, 2H, J = 2.7 Hz), 8.10 (dd, 1H, J = 2.1, 7.2 Hz), 8.30 (d, 1H, J = 9 Hz), 8.63 (d, 1H, J = 2.1 Hz), 9.47(dt, 2H, J = 0.9, 5.4 Hz), 9.80 (m, 2H) ppm. Anal. Calcd for $C_{21}H_9N_4BrClO_3Re$: C, 37.82; H, 1.36; N, 8.40; Br, 11.98; Cl, 5.32. Found: C, 37.96; H, 1.45; N, 8.23; Br, 12.12; Cl, 5.39.

Solid-State Structures. Crystals of complexes **7** and **8** were grown from a concentrated dichloromethane solution, and X-ray crystallographic data were collected at −97 or −109 °C, respectively, on a Siemens SMART system using graphite monochromated Mo Kα radiation with exposures over 0.3°. No appreciable decay of the crystals was detected during data collection. Data were corrected for Lorentz and polarization effects using SAINT.[34] The structures were solved by direct methods using SIR-97[35] running within the WinGX package,[36] with the resulting Fourier map revealing the location of all non-hydrogen atoms. A weighted full-matrix refinement on F^2 was carried out using SHELXL-97,[37] with all non-hydrogen atoms being refined anisotropically for **7** and **8**. Hydrogen atoms were included in calculated positions and were refined as riding atoms with individual (or group, if appropriate) isotropic displacement parameters. A possible disorder of C(30) in **7** was evidenced by large thermal parameters, but this was not investigated further. The bromine atom in **8** was found to be disordered over two sites, and this was modeled successfully using a 50:50 occupancy. This, of course, means that the entire ligand must be disordered over two sites, and such disorder is perhaps suggested by the elongated ellipsoids of the bromine-substituted ring. However, all attempts to model the disorder of the entire ligand resulted in numerous atoms displaying nonpositive definite thermal parameters, and thus, this disorder was not examined further.

Computational Studies. The Gaussian 03W package[38] was used to carry out geometry optimizations and frequency calculations for compounds **1**−**8**. The geometry optimizations, vibrational frequencies, and their IR and Raman intensities were calculated using DFT (B3LYP/6-31G(d)). Rhenium(I) and ruthenium(II) centers were represented using the effective core potential and associated LANL2DZ basis set. The optimized structure was used to calculate vibrational frequencies. Importantly, none of the frequency calculations generated imaginary frequencies; this is consistent with an energy minimum for the optimized geometry.

Electroluminescence Studies. OLEDs were fabricated by deposition onto an indium tin oxide (ITO) glass substrate. The ITO (R_s = 100 Ω/square) was patterned by etching with 37% HCl/$FeCl_3$ and cleaned using acetone and Opti-Clean (Datronix) optical cleaning polymer.

A solution of N,N′-diphenyl-N,N′-di(3-methylphenyl)benzidine (TPD) (Aldrich) in 1,1,2-trichloroethane (10 mg/mL) was spin coated onto ITO as a hole transport layer. The emitting layer containing poly(vinylcarbazole) (PVK; 10 mg/mL), TPD (1 mg/mL), 2-[1,1′-biphenyl]-4-yl-5-[4-(1,1-dimethylethyl)phenyl]-1,3,4-oxadiazole (from Aldrich; 4 mg/mL), and the dopant (0.5 mg/mL) in 1,1,2-trichloroethane was spin coated over the hole transport layer. Some washing away of the hole transport layer is expected.

(34) *SAINT*, version 4; Siemens Analytical X-ray Systems: Madison, WI, 1996.
(35) Altomere, A.; Burla, M. C.; Camilla, M.; Cascarano, G. L.; Giacovazzo, C.; Guagliardi, A.; Moliterni, A. G. G.; Polidori, G.; Spagna, R. *J. Appl. Crystallogr.* **1999**, *32*, 115.
(36) Farrugia, L. J. *J. Appl. Crystallogr.* **1999**, *32*, 837.
(37) Sheldrick, G. M. *SHELXL-97*; University of Göttingen: Göttingen, Germany, 1997; Program for the Refinement of Crystal Structures section.
(38) Frisch, M. J.; Trucks, G. W.; Schlegel, H. B.; Scuseria, G. E.; Robb, M. A.; Cheeseman, J. R.; Montgomery, J. J. A.; Vreven, T.; Kudin, K. N.; Burant, J. C.; Millam, J. M.; Iyengar, S. S.; Tomasi, J.; Barone, V.; Mennucci, B.; Cossi, M.; Scalmani, G.; Rega, N.; Petersson, G. A.; Nakatsuji, H.; Hada, M.; Ehara, M.; Toyota, K.; Fukuda, R.; Hasegawa, J.; Ishida, M.; Nakajima, T.; Honda, Y.; Kitao, O.; Nakai, H.; Klene, M.; Li, X.; Knox, J. E.; Hratchian, H. P.; Cross, J. B.; Adamo, C.; Jaramillo, J.; Gomperts, R.; Stratmann, R. E.; Yazyev, O.; Austin, A. J.; Cammi, R.; Pomelli, C.; Ochterski, J. W.; Ayala, P. Y.; Morokuma, K.; Voth, G. A.; Salvador, P.; Dannenberg, J. J.; Zakrzewski, V. G.; Dapprich, S.; Daniels, A. D.; Strain, M. C.; Farkas, O.; Malick, D. K.; Rabuck, A. D.; Raghavachari, K.; Foresman, J. B.; Ortiz, J. V.; Cui, Q.; Baboul, A. G.; Clifford, S.; Cioslowski, J.; Stefanov, B. B.; Liu, G.; Liashenko, A.; Piskorz, P.; Komaromi, I.; Martin, R. L.; Fox, D. J.; Keith, T.; Al-Laham, M. A.; Peng, C. Y.; Nanayakkara, A.; Challacombe, M.; Gill, P. M. W.; Johnson, B.; Chen, W.; Wong, M. W.; Gonzalez, C.; Pople, J. A. *Gaussian 03*, revision B.04; Gaussian, Inc.: Pittsburgh, PA, 2003.

Table 1. Crystallographic Data for **7** and **8**

	7	**8**
formula	$C_{24}H_{14}ClN_4O_5Re$	$C_{44}H_{24}Br_2Cl_2N_8O_8Re_2$
fw	660.04	1395.83
space group	$P\bar{1}$	$C2/c$
Z	2	4
cryst syst	triclinic	monoclinic
a (Å)	6.403(5)	19.506(5)
b (Å)	10.388(5)	18.043(5)
c (Å)	16.976(5)	13.320(5)
α (deg)	84.087(5)	
β (deg)	84.161(5)	114.936(5)
γ (deg)	79.369(5)	
V, Å^3	1099.9(11)	4251(2)
D calcd (g cm^{-3})	1.993	2.181
temp (°C)	−97	−109
λ, (Å)	0.710 69	0.710 69
μ (mm^{-1})	5.692	7.762
R1	0.0536	0.0298
wR2	0.0932	0.0827

Table 2. Selected Bond Lengths (Å) and Angles (deg) for **7** and **8**

7

Re(1)−N(1)	2.170(6)	Re(1)−C(1)	1.921(8)
Re(1)−N(2)	2.185(5)	Re(1)−C(2)	1.927(8)
Re(1)−Cl(1)	2.4683(19)	Re(1)−C(3)	1.890(8)
N(1)−Re(1)−N(2)	75.6(2)	N(2)−Re(1)−C(3)	94.1(2)
N(1)−Re(1)−Cl(1)	83.12(16)	Cl(1)−Re(1)−C(1)	93.3(2)
N(1)−Re(1)−C(1)	97.2(3)	Cl(1)−Re(1)−C(2)	91.1(2)
N(1)−Re(1)−C(2)	172.6(3)	Cl(1)−Re(1)−C(3)	177.1(2)
N(1)−Re(1)−C(3)	95.8(2)	C(1)−Re(1)−C(2)	87.5(3)
N(2)−Re(1)−Cl(1)	83.12(16)	C(1)−Re(1)−C(3)	89.4(3)
N(2)−Re(1)−C(1)	172.3(3)	C(2)−Re(1)−C(3)	90.0(3)
N(2)−Re(1)−C(2)	99.4(3)		

8

Re(1)−N(1)	2.171(4)	Re(1)−C(100)	1.911(5)
Re(1)−N(2)	2.168(4)	Re(1)−C(200)	1.902(6)
Re(1)−Cl(1)	2.4648(15)	Re(1)−C(300)	1.900(6)
N(1)−Re(1)−N(2)	75.21(15)	N(2)−Re(1)−C(300)	175.1(2)
N(1)−Re(1)−Cl(1)	80.51(11)	Cl(1)−Re(1)−C(100)	96.14(16)
N(1)−Re(1)−C(100)	171.51(17)	Cl(1)−Re(1)−C(200)	176.46(19)
N(1)−Re(1)−C(200)	96.0(2)	Cl(1)−Re(1)−C(300)	91.8(2)
N(1)−Re(1)−C(300)	101.4(2)	C(100)−Re(1)−C(200)	87.3(2)
N(2)−Re(1)−Cl(1)	84.26(11)	C(100)−Re(1)−C(300)	86.4(2)
N(2)−Re(1)−C(100)	96.76(18)	C(200)−Re(1)−C(300)	89.4(3)
N(2)−Re(1)−C(200)	94.4(2)		

Thermal evaporation at a pressure of 0.01 mTorr was used to deposit a layer of 2,9-dimethyl-4,7-diphenyl-1,10-phenanthroline to a thickness of approximately 6 nm, and tris(8-hydroxyquinolinate)aluminum (Alq_3) was deposited to a thickness of 20 nm. This was followed by deposition of the aluminum cathode, at a thickness of 200 nm. The thickness of the layers was monitored using a Taylor−Hobson Talystep mechanical probe.

Emission spectra were obtained on a Perkin-Elmer LS-50B fluorescence spectrometer. A luminance meter (Topcon BM-9) was used to measure the brightness of the devices, and the current was monitored with a Fluke multimeter.

Results and Discussion

Structural Studies. X-ray data for **7** and **8** are presented in Table 1, and selected bond lengths and angles are shown in Table 2. ORTEP diagrams of the two structures are presented in Figure 2. A labeled diagram of **1** is shown in Figure 1. The rhenium−ligand bond lengths of **7** are comparable to those observed in the similar complexes *fac*-[Re(1,10-phenanthroline)$(CO)_3$Cl][39] and *fac*-[Re(dipyrido-[2,3-*a*:3′,2′-*c*]phenazine)$(CO)_3$Cl].[40] The geometry about

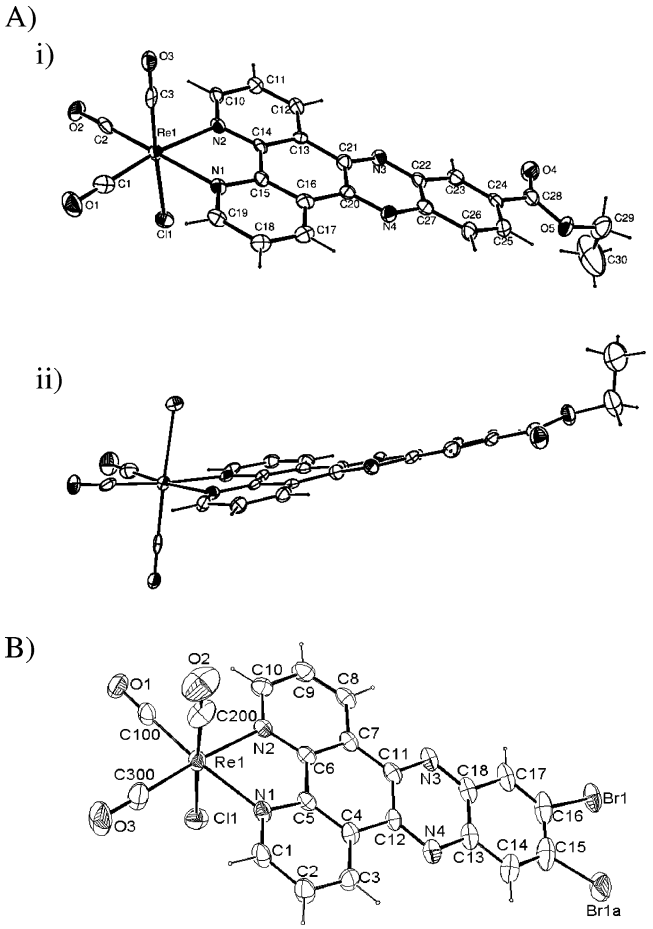

Figure 2. (A) (i) ORTEP view of **7** with atom labeling scheme. (ii) Alternative view of **7** emphasizing distortion of the dppz ligand. (B) ORTEP view of **8** showing the disorder of the bromine atom over two sites (50:50 occupancy). Ellipsoids are drawn at the 30% probability level in all cases.

Re(1) is distorted octahedral because of a N(1)−Re(1)−N(2) bond angle of 75.6(2)°.

A comparison of the solid-state structure of **7** with the structure obtained from DFT calculations shows close agreement between the calculated and experimentally observed bond lengths (Table 3). The difference between bond lengths within the crystal and calculated structures of **7** is less than 0.02 Å. This contrasts with a comparison of calculations performed on the dppz ligand using B3LYP/6-31G(d)[41] and crystallographic data for [Ru(bpy)$_2$(11,12-dimethyldipyrido[3,2-*a*:2′,3′-*c*]pyridine)](ClO$_4$)$_2$[42] and [Pt-(dppz)(2,4,6-trimethylphenyl)$_2$]·toluene,[16] which showed a large number of bond lengths differing from the calculated values by more than 0.03 Å.

The dppz ligand in the complexes [Re(I)(dppz)(4-methylpyridine)$(CO)_3$](OTf)[4] and [Re(benzo[*i*]dipyrido[3,2-*a*:2′,3,-*c*]phenazine)$(CO)_3$(pyridine)](OTf)[43] is essentially

(39) Haddad, S. F.; Marshall, J. A.; Crosby, G.; Twamley, B. *Acta Crystallogr., Sect. E* **2002**, *E58*, m559.
(40) Polson, M. I. J.; Howell, S. L.; Flood, A. H.; Burrell, A. K.; Blackman, A. G.; Gordon, K. C. *Polyhedron* **2004**, *23*, 1427.
(41) Matthewson, B. J.; Flood, A.; Polson, M. I. J.; Armstrong, C.; Phillips, D. L.; Gordon, K. C. *Bull. Chem. Soc. Jpn.* **2002**, *75*, 933.
(42) Komatsuzaki, N.; Katoh, R.; Himeda, Y.; Sugihara, H.; Arakawa, H.; Kasuga, K. *J. Chem. Soc., Dalton Trans.* **2000**, 3053.
(43) Yam, V. W.-W.; Lo, K. K.-W.; Cheung, K.-K.; Kong, R. Y.-C. *J. Chem. Soc., Chem. Commun.* **1995**, 1191.

Table 3. Selected Calculated and Observed Bond Lengths of Ligands and Complexes

compound; bond parameter[a]	**1**; 6-31G(d)[b]	**3**; 6-31G(d)	**5**; 6-31G(d), LANL2DZ	**7**; 6-31G(d), LANL2DZ	**7**; crystal structure	**2**; 6-31G(d)	**4**; 6-31G(d)	**6**; 6-31G(d), LANL2DZ	**8**; crystal structure	**8**; 6-31G(d), LANL2DZ	**9**; crystal structure
r_2	1.383	1.386	1.386	1.386	1.367	1.383	1.386	1.386	1.352	1.385	1.370
r_2'	1.383	1.386	1.386	1.386	1.352	1.383	1.386	1.386	1.365	1.385	1.337
r_3	1.404	1.399	1.400	1.398	1.389	1.404	1.399	1.400	1.398	1.398	1.356
r_4	1.328	1.338	1.340	1.338	1.327	1.328	1.338	1.340	1.323	1.338	1.376
r_5	1.347	1.359	1.365	1.359	1.367	1.347	1.359	1.365	1.347	1.358	1.356
r_6	1.415	1.407	1.408	1.407	1.396	1.415	1.407	1.408	1.394	1.407	1.383
r_7	1.476	1.458	1.449	1.453	1.448	1.476	1.458	1.449	1.442	1.452	1.424
r_8	1.462	1.463	1.463	1.463	1.461	1.462	1.463	1.463	1.445	1.463	1.448
r_9	1.440	1.434	1.432	1.438	1.429	1.440	1.433	1.431	1.426	1.438	1.421
r_{11}	1.353	1.351	1.349	1.352	1.350	1.352	1.351	1.350	1.348	1.351	1.336
r_{12}	1.434	1.441	1.446	1.437	1.415	1.434	1.441	1.445	1.408	1.436	1.468
Δ_r	0.1	0.1	0.1	0.1	0.8	0.0	0.1	0.1	0.6	0.0	2.6
r_{15}	1.427	1.428	1.429	1.427	1.420	1.421	1.425	1.428	1.405	1.423	1.396
r_{16}	1.494	1.501	1.504	1.496	1.482	1.909	1.897	1.890	1.834	1.903	
r_{18}	1.349	1.342	1.338	1.346	1.337						
r_{19}	1.447	1.454	1.458	1.449	1.442						
r_{20}	1.517	1.516	1.515	1.517	1.402						
ϕ_1	119.1	119.1	119.1	118.9	119.3	119.1	119.1	119.1	119.4	119.0	118.9
ϕ_1'	119.1	119.1	119.1	119.0	120.7	119.1	119.1	119.1	118.8	119.0	119.8
ϕ_4	118.2	118.1	118.4	118.5	118.5	118.1	118.1	118.5	119.0	118.6	116.9
ϕ_4'	118.2	118.1	118.4	118.6	118.3	118.1	118.1	118.4	117.5	118.6	120.3
ϕ_5	122.3	122.6	122.4	122.3	122.1	122.3	122.6	122.4	122.2	122.3	123.6
ϕ_5'	122.3	122.6	122.4	122.3	122.8	122.3	122.6	122.4	123.2	122.3	121.2
ϕ_9	119.6	119.8	119.8	119.8	119.2	119.5	119.7	119.8	120.2	119.7	118.8
ϕ_9'	119.5	119.7	119.8	119.7	120.6	119.6	119.8	119.9	119.4	119.8	120.5
Δ_ϕ	0.1	0.1	0.1	0.1	0.6	0.3	0.2	0.2	0.6	0.3	1.2

[a] Bond lengths (r) in Å, average difference in bond lengths about C_{2v} axis (Δ_r) in pm; bond angles (ϕ) in degrees, average difference in bond angles about C_{2v} axis (Δ_ϕ) in degrees. [b] Basis sets used in geometry calculations.

planar, showing mean deviations of 0.019 Å (maximum deviation = 0.1174 Å) and 0.0084 Å (maximum deviation = 0.1104 Å), respectively, from the least-squares plane of N4, N5, C11, and C12 (Figure 1). However, the dppz ligand in **7** was found to be significantly distorted (Figure 2) with deviations from the least-squares plane of the atoms N(1), N(2), C(24), and C(25) of up to 0.2537 Å for N(4) and a mean deviation of 0.0578 Å. Ligand distortion in dppz-based complexes has been previously observed in crystal structures of [Ru(dppz)(2,9-dimethyl-1,10-phenanthroline)$_2$](PF$_6$)$_2$,[44] [Cu(dppz)(tris(3-phenylpyrazolyl)borate)](ClO$_4$),[45] and [Os$_4$(dppz)(μ-H)$_4$(CO)$_{10}$].[46] Similar distortion has been observed for other polypyridyl ligands in rhenium(I) complexes such as [Re(dipyrido[2,3-*a*:3′,2′-*c*]phenazine)(CO)$_3$Cl].[40] For this complex, it was suggested that a destabilizing steric interaction between equatorial carbonyls and protons ortho to the nitrogen donors caused distortion of the polypyridyl ligand. It is unlikely that this is the case for **7**, as the C(1)−H(19) distance of 2.812 Å and the C(2)−H(10) distance of 2.936 Å are similar to the distances for the complexes [Re(I)(dppz)(4-methylpyridine)(CO)$_3$](OTf) (2.724 and 2.950 Å)[4] and [Re(benzo[*i*]dipyrido[3,2-*a*:2′,3,-*c*]phenazine)(CO)$_3$(pyridine)](OTf) (2.919 and 2.801 Å)[43] in which the dppz ligands are approximately planar. The distortion of the dppz ligand in **7** may instead be a combination of crystal packing effects and $\pi-\pi$ stacking interactions between the dppz ligands (Figure 3). The optimized geometries of **7** and **8** as calculated by density functional theory display a planar aromatic backbone of dppz because crystal packing forces are not considered in calculations performed on single molecules.

The geometry about the rhenium atom in **8** is similar to that of **7**. The N(1)−Re(1)−N(2) bond angle of 75.21(15)° again leads to a distorted octahedral geometry. The Re−C, Re−N, and Re−Cl bond lengths of **8** are comparable to those of **7** and other similar complexes. The differences in corresponding bond lengths between the solid-state and calculated geometries of **8** are similar to the differences observed for **7**. Disagreements between observed and calculated bond lengths of **8** are generally less than 0.02 Å. Complex **8** also shows distortion of the backbone of the dppz-based ligand, with deviations from the least-squares plane of N(1), N(2), C(15), and C(16) of up to 0.1877 Å for N(3) and a mean deviation of 0.0536 Å. The distortion of the dppz-based ligand in **8** allows the formation of isomers in the solid state because it causes the two possible orientations of the ligand to become nonequivalent. Refinement of the occupancies of these two isomers shows them to be present in an essentially 1:1 ratio (0.50063:0.49937). The isomers are not resolved in solution by ^{1}H NMR spectroscopy, implying that the ligand distortion observed in the solid-state structure is either not present or not fixed in solution. The distances of the ortho hydrogen atoms from the nearest carbonyl carbon are 2.772 Å [C(100) and H(10)] and 2.970 Å [C(300) and H(1)], similar to that observed for the crystal structure of **7**, suggesting that the ligand distortion again does not arise because of a steric interaction between the carbonyl ligands and the dppz-based ligand. Complex **8** shows strong $\pi-\pi$ stacking interactions, which may account

(44) Liu, J.-G.; Zhang, Q.-L.; Shi, X.-F.; Ji, L.-N. *Inorg. Chem.* **2001**, *40*, 5045.
(45) Dhar, S.; Reddy, P. A. N.; Nethaji, M.; Mahadevan, S.; Saha, M. K.; Chakravarty, A. R. *Inorg. Chem.* **2002**, *41*, 3469.
(46) Choi, Y.-Y.; Wong, W.-T. *J. Organomet. Chem.* **1999**, *573*, 189.

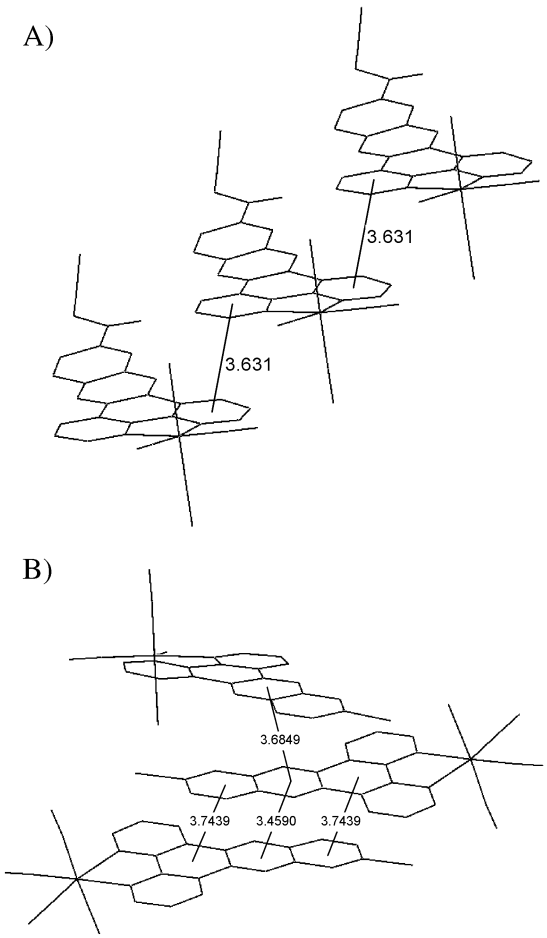

Figure 3. $\pi-\pi$ stacking interactions of **7** (A) and **8** (B) showing centroid−centroid distances (Å). Hydrogen atoms and solvent molecules have been omitted for clarity.

for the distortion of the dppz skeleton (Figure 3). The ligands π-stack in an alternating fashion with an average centroid−centroid distance of 3.6489 Å.

Calculated Structural Data. The calculated structures offer some insight into the effects of metal bonding and ligand conformation. Rotation about bond r_{16} allows the possibility of two conformational isomers for **1** that lie at local energy minima. It is possible to model this isomerization using computational methods. B3LYP/6-31G(d) calculations on each conformer of **7** showed the trans conformer, in which r_{14} is trans to r_{17}, to be 1.7 kJ mol^{-1} lower in energy than the cis conformer. Because these two rotational conformers lie close in energy, structures and spectra were calculated for the trans conformer, although the obtained crystal structure of **7** showed the presence of the cis conformer only.

The calculated structural parameters for **1**−**8** are compared with the crystallographic data in Table 3. A comparison of calculated optimized structures for **1**−**8** shows that the ligand structure is calculated to be sensitive to different metal centers. Binding of **1** or **2** to a rhenium(I) center produces calculated bond length changes relative to the free ligand of more than 0.01 Å in the phenanthroline section of the ligand. However, binding to a ruthenium(II) center generates predicted bond length changes relative to the free ligand of more than 0.01 Å along the phenazine backbone and ester functionality. Binding to a copper(I) center produces moderate (0.005−0.010 Å) bond length changes along the phenazine backbone and ester bonds. These findings are consistent with the weak effect the $\{Cu(PPh_3)_2\}^+$ fragment is known to have on the structure of bound ligands.[17]

Table 4. Electronic Absorption Data for Ligands and Complexes

	absorption λ_{max}/nm[a] ($\epsilon \times 10^{-4}$/mol^{-1} L cm^{-1})		
	$\pi^* \leftarrow \pi$	mixed	MLCT
1	276(3.02)		
	348(0.53)		
	356(0.60)		
	366(0.82)		
	374(0.67)		
	386(0.81)		
2	279(2.83)		
	329(0.70)		
	366(0.61)		
	385(0.68)		
3[b]	280(9.15)	381(1.19)	
	334(1.84)		
	362(1.35)		
4[b]	282(6.03)	385(1.39)	
	330(1.00)		
	366(1.20)		
5	283(12.1)		442(1.75)
	362(1.88)		
6	284(8.42)		441(1.31)
	364(1.25)		
	375(1.55)		
7	281(14.0)	363(2.44)	
	323(2.88)		
8	283(4.01)	384(1.05)	
	321(1.23)		
	367(1.11)		

[a] Spectra were recorded in dichloromethane unless otherwise stated. [b] Recorded in acetonitrile.

Electronic Absorption Spectra. The UV−visible spectral data of **1**−**8** are presented in Table 4. The ligands both show typical absorption spectra for 11-substituted dppz ligands[18] with an intense transition at approximately 280 nm and a series of weaker bands in the 360 nm region. On the basis of the similarity of the spectra of **1** and **2** to those of other ligands of this type, the bands at 280 and 360 nm are assigned as LC transitions. Complexation of **1** or **2** to a metal center results in a red shift of the LC transition. The LC transitions for **2** and its complexes occur at slightly lower energy than for **1** and its corresponding complexes in all cases. Because substitution of the ligand affects the position of the LC transition, an orbital involved in this transition is phz-based. The complexes absorb weakly in the visible region, with patterns similar to those of other complexes of the type.[14] The ruthenium complexes show MLCT bands at around 440 nm, due to the known chromophore Ru(II) → bpy,[47] whereas the copper and rhenium complexes have their higher-energy MLCT transitions overlapped by the more-intense LC transition. The MLCT shoulder of **7** extends further into the visible region than for **8**.

Electrochemical Studies. Electrochemical data for compounds **1**−**8** are presented in Table 5. Substitution of dppz with an ester group or bromine substituent results in reduction

(47) Hartshorn, R. M.; Barton, J. K. *J. Am. Chem. Soc.* **1992**, *114*, 5919.

Table 5. Electrochemical Data for Ligands and Complexes

compound	E^0/V[a] reduction	compound	E^0/V[a] reduction
1	−1.07	**5**	−0.77
2	−1.11	**6**	−0.86
3	−0.85	**7**	−0.82
4	−0.95	**8**	−0.87

[a] Reduction potentials of compounds **1**, **2**, **7**, and **8** were recorded in dichloromethane with the decamethylferrocene/decamethylferrocenium couple as a reference. Compounds **3**−**6** had their reduction potentials recorded in acetonitrile. 0.1 M tetrabutylammonium perchlorate was used as the supporting electrolyte in all cases.

Table 6. Fluorescent Maxima and Excited-State Lifetimes of Ligands and Complexes

compound	excited-state absorption λ_{max}/nm[a]	τ/μs
1	446	not determined
2	453	not determined
3[b]	443, 605	1.06
4[b]	650	2.25
5	622	0.27
6	652	0.24
7	432	1.01
8	456	1.57

[a] Fluorescence and lifetime measurements were performed in dichloromethane unless otherwise stated. [b] Recorded in acetonitrile.

occurring at less-negative potentials than for unsubstituted dppz (−1.60 V vs Fc^+/Fc).[14] Coordination of the ligands to a metal center also causes reductions to occur at less negative potentials. It is generally found that, for metal polypyridyl complexes, the stabilization of the first ligand-based reduction potential ($E^{o/}$[first reduction of the free ligand] − $E^{o/}$[first reduction of the metal complex]) is greater for Ru(II) and Re(I) than for Cu(I).[18] This is found to occur for complexes of **1** and **2**. This is a surprising result as unsubstituted dppz complexes show very little change in reduction potential as a function of the chelating metal center.[14] This has been rationalized in terms of the reducing electron for dppz complexes causing structural distortions over the phenazine portion of the dppz ligand and not affecting the phenanthroline section. In terms of a MO picture of the reduction process, the reducing electron may be thought of as occupying a redox MO,[48] which has considerable phenazine character. The tuning of the reduction potential with 11-position substitution *and* metal binding does not fit within the confines of the Kaim MO model[12−16] and suggests that the reduction is not partitioned in the fashion inferred from data on unsubstituted dppz.

Fluorescence and Lifetime Studies. The fluorescence and lifetime measurements are presented in Table 6. The free ligands displayed fluorescence at around 450 nm, values consistent with other 11-substituted dppz ligands.[18] All of the complexes are fluorescent, and their behavior may be divided into three categories. Complexes **7** and **8** are fluorescent at a similar wavelength to that of the free ligand, suggesting that the emissions from **7** and **8** are LC in nature. Complexes **4**, **5**, and **6** displayed fluorescent maxima at lower energy, suggesting that the presence of a metal ion can affect the emission wavelength. Complex **3** was emissive at two wavelengths, one similar to that of the free ligand and the other at a longer wavelength.

The ruthenium complexes, **5** and **6**, displayed the shortest excited-state lifetimes. These were similar, which suggests that substitution of the 11-position of dppz has little effect on the dynamics of these excited states. The emission maxima are shifted by 30 nm on going from **5** to **6**.

It is typical for the MLCT excited states of rhenium complexes to show dynamic behavior dominated by the energy-gap law.[49] The absorption of light by **7** extends to lower energy than **8**, implying a lower-lying MLCT state for **7**. The electrochemical data show that **7** is 50 mV easier to reduce than **8**, and the fact that the excited-state lifetime of **7** is shorter than that of **8** is consistent with these findings.

The copper complexes display by far the most interesting excited-state properties. The excited-state lifetimes of the complexes in dichloromethane are comparatively long but completely quenched if the solvent is changed to methanol. This marked solvent dependence suggests that the excited states of **3** and **4** are MLCT in nature, as copper(I) complexes that emit from MLCT excited states are strongly solvent-dependent.[17] For copper(I) complexes, the main influence on the excited-state lifetime is its ability to form a solvent-based exciplex with increased steric protection, thereby prolonging the lifetime.[50] The long lifetimes of **3** and **4** suggest that the solvent-based exciplexes are relatively stable for an excited state in a nonprotic solvent such as dichloromethane. Although this result is surprising, it is consistent with electrochemical data.

Vibrational Spectra. The efficacy of the calculations for those complexes for which structural data are not available may be tested by using the calculations to predict other observables of the complexes. The vibrational spectra offer an opportunity to compare calculated and experimental parameters. Experimental and calculated Raman spectra for **7** are presented in Table 7, along with experimental and calculated IR spectra and assignments of vibrational modes. A comparison of the calculated and experimental spectra shows good correlation. Bands in the IR and Raman spectra between 1000 and 1650 cm^{-1}, with a relative intensity (RI) of at least 25% of the most intense band, have an absolute mean deviation of less than 6 cm^{-1} for compounds **1**−**8**. The carbonyl band is not as well-predicted by the calculations as the other modes;[51] however, it is easily identifiable as a strong band at about 1700 cm^{-1} (mode 124 for **7**: calcd, 1756 cm^{-1}; exptl, 1708 cm^{-1}). Figure 4 shows experimental and calculated IR and Raman spectra for **6**. A comparison of the experimental and calculated spectra for **6** shows good agreement, with an absolute mean deviation for bands with RI 25% of 5 cm^{-1}. The FT-IR spectrum shows five strong peaks between 1400 and 1500 cm^{-1}, which are reproduced

(48) De Armond, M. K.; Myrick, M. L. *Acc. Chem. Res.* **1989**, *22*, 364.
(49) Caspar, J. V.; Meyer, T. J. *J. Phys. Chem.* **1983**, *87*, 952.
(50) McMillin, D. R.; Gamache, R. E., Jr; Kirchoff, J. R. *Copper Coordination Chemistry: Biochemical and Inorganic Perspectives*; Adenine Press: New York, 1983.
(51) This is, in part, due to the greater anharmonicity of the CO modes versus the polypyridyl ligand modes for which the scaling factor is optimized

Table 7. Calculated and Experimental Frequencies (cm^{-1}) and Relative IR and Raman Intensities for Selected Normal Modes of **7** and **8**

mode[a]	major bonds involved[b]	ν/cm^{-1} calcd	(int.)[c]	ν/cm^{-1} exptl	(int.)[c]
	7				
92	$r_{11} - r_1 - r_1'$	1193	(9, 3)	1182	(0, 6)
93	$r_5 + r_8' + r_{10}' - r_8 - r_{11} - r_{18}$	1216	(39, 2)	1209	(41, 4)
102	$r_7 - r_4 - r_4'$	1325	(2, 27)	1316	(4, 77)
103	$r_9 - r_8 - r_8' - r_{12}$	1353	(23, 20)	1347	(0, 18)
104	$r_{10} + r_{10}' + r_{12} - r_9$	1356	(18, 1)	1358	(50, 17)
106	$r_{12} + r_{14} + r_{14}' - r_{13} - r_{13}$	1410	(4, 100)	1409	(55, 93)
107	r_{20}	1418	(8, 7)	1416	(71, 100)
109	$r_6 + r_6' - r_7$	1444	(7, 7)	1445	(38, 80)
111	$r_5 + r_8 + r_{13}' - r_1 - r_7$	1479	(2, 3)	1472	(0, 1)
114	r_{20}	1490	(1, 1)	1494	(6, 22)
117	$r_{10} + r_{11}' - r_{10}' - r_{11}$	1552	(1, 8)	1536	(1, 26)
119	$r_6 + r_6' - r_2 - r_2'$	1585	(0, 0)	1574	(9, 1)
120	$r_2 + r_2' - r_1 - r_1'$	1597	(1, 12)	1594	(0, 59)
	8				
78	$r_7 + r_{11} - r_1 - r_1'$	1193	(5,2)	1183	(9,3)
79	$r_5 + r_8' - r_5' - r_8'$	1217	(3,0)	1212	(9,2)
82	$r_5 + r_5' - r_7$	1282	(3,6)	1279	(0,2)
85	$r_5 + r_8 - r_2 - r_4$	1316	(5,3)	1316	(0,53)
87	$r_8 + r_8' - r_{10} - r_{10}'$	1351	(4,9)	1344	(0,7)
88	$r_9 - r_{12}$	1352	(100,7)	1357	(74,7)
89	$r_{12} + r_{14} + r_{14}' - r_{13} - r_{13}'$	1405	(6, 100)	1405	(0,100)
90	$r_6' + r_{10} - r_6 - r_{13}$	1418	(35,1)	1413	(78,0)
91	$r_6 + r_6' - r_7$	1443	(3,9)	1446	(48,49)
92	$r_1' + r_{11} - r_8 - r_{13}$	1454	(29,7)	1463	(34,0)
95	$r_8 + r_{15} - r_3' - r_7 - r_{13}'$	1495	(58,3)	1491	(100,9)
96	$+ r_{14} + r_{14}' - r_{12} - r_{15}$	1547	(4,0)	1538	(0,14)
98	$r_6 + r_6' - r_2 - r_2'$	1584	(0,1)	1577	(0,2)
99	$r_1 + r_1' + r_4' + r_7 - r_3'$	1597	(4,9)	1595	(45,44)
102	$r_6 + r_{13}' + r_{14} - r_6' - r_{13} - r_{14}'$	1621	(30,2)	1617	(12,7)

[a] Mode numbers for **7** and **8**. [b] Main bond stretches that are involved in the mode of vibration. [c] Relative intensities for IR and Raman bands, respectively, normalized so that the most intense band in the reported spectral region is equal to 100.

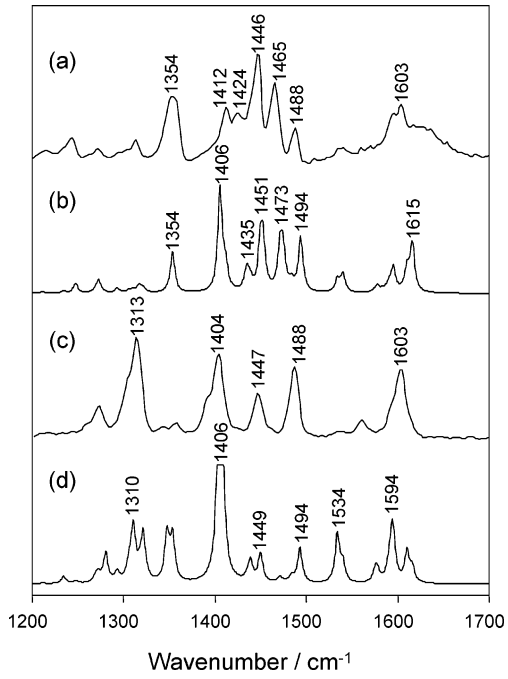

Figure 4. Vibrational spectra for **6**: (a) FT-IR spectrum (KBr disk), (b) calculated IR spectrum, (c) FT-Raman spectrum, and (d) calculated Raman spectrum.

in the calculated IR spectrum in the same region. The 1488 cm^{-1} band is predicted at 1494 cm^{-1} and also appears in the Raman spectrum. A feature at 1354 cm^{-1} also appears in both the experimental and calculated IR spectra. The FT-Raman spectrum has a band and shoulder at 1310 cm^{-1}, which appears in the calculated Raman spectrum as two bands. A broad band at 1604 cm^{-1} may conceal a shoulder at 1616 cm^{-1}. Table 7 shows the experimental and calculated FT-IR and FT-Raman spectral data of **8** with assigned vibrational modes. A comparison of the calculated and experimental spectra of **8** shows good correlation, with an absolute mean deviation for bands with RI 25% of 5 cm^{-1}. In all DFT calculations on **3**−**8**, an unusually large intensity was predicted for a vibrational mode due to the phz stretch at about 1410 cm^{-1}. The increased intensity of this band is not reflected in the experimental data or the calculated IR spectrum. In the Raman spectrum of **6**, the predicted band at 1406 cm^{-1} shows an intensity relative to the 1310 cm^{-1} band of 4:1; experimentally, this value is closer to 0.8:1 (Figure 4). This finding is not without precedent; in a study of substituted terthiophene compounds, Casado et al.[52] found that the strongest predicted band at 1393 cm^{-1} was almost 5 times more intense than that observed in the experimental data.

Electro-Optical Properties. The development of electroluminescent (EL) systems based on conducting polymers and inorganic components has led to much research into materials for display and lighting technologies.[53−55] The design of such materials can lead to improved efficiency, color tuning, and an increased lifetime of EL displays. The incorporation of metal polypyridyl complexes into electroluminescent systems has resulted in interesting developments for the technology.

Phosphorescent (triplet) emitters such as Ru(II) and Re(I) polypyridyl complexes have an advantage over fluorescent (singlet) emitters,[56] as only 25% of the excitons formed in the EL process are singlets.[57] This means that fluorescent emitters have an absolute efficiency limit of 25%. Incorporating some Ru(II) complexes into organic polymers also increases charge mobility in the polymer film because the Ru(II) complex acts as a charge carrier.[58] Das et al.[59] studied the electrophosphorescence of $Ir(Me\text{-}ppy)_3$, a triplet emitter (Me-ppy = 3-methyl-2-phenylpyridine). Methyl substitution at the 3-position influences the extent of delocalization between the pyridyl and phenyl rings. This allows fine tuning of the energy levels of ppy MOs, which gives a color-tuning capability. Studies of electroluminescent systems containing *fac*-$[Re(CO)_3Cl(pp)]$ and $[Ru(bpy)_2(pp)]^{2+}$ complexes, where (pp) is a polypyridyl ligand with triphenylamine and oxa-

(52) Casado, J.; Pappenfus, T. M.; Mann, K. R.; Orti, E.; Viruela, P. M.; Milian, B.; Hernandez, V.; Navarrete, J. T. L. *ChemPhysChem* **2004**, *5*, 529.
(53) Yu, J.-S. K.; Chen, W.-C.; Yu, C.-H. *J. Phys. Chem. A* **2003**, *107*, 4268.
(54) Lee, C.-L.; Lee, K. B.; Kim, J.-J. *Appl. Phys. Lett.* **2000**, *77*, 2280.
(55) Drolet, N.; Beaupre, S.; Morin, J.-F.; Tao, Y.; Leclerc, M. *J. Opt. A: Pure Appl. Opt.* **2002**, *4*, S252.
(56) Lamansky, S.; Kwong, R. C.; Nugent, M.; Djurovich, P. I.; Thompson, M. E. *Org. Electron.* **2001**, *2*, 53.
(57) Baldo, M. A.; O'Brien, D. F.; Thompson, M. E.; Forrest, S. R. *Phys. Rev. B: Condens. Matter Mater. Phys.* **1999**, *60*, 14422.
(58) Chan, W. K.; Ng, P. K.; Gong, X.; Hou, S. *J. Mater. Chem.* **1999**, *9*, 2103.
(59) Das, R. R.; Lee, C.-L.; Noh, Y.-Y.; Kim, J.-J. *Opt. Mater. (Amsterdam, Neth.)* **2003**, *21*, 143.

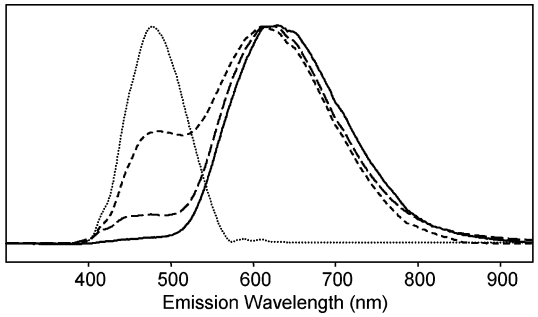

Figure 5. Emission profile for EL devices containing complex **7** at 3 wt % (solid line), 0.7 wt % (long dashed line), 0.07 wt % (short dashed line), and 0.007 wt % (dotted line).

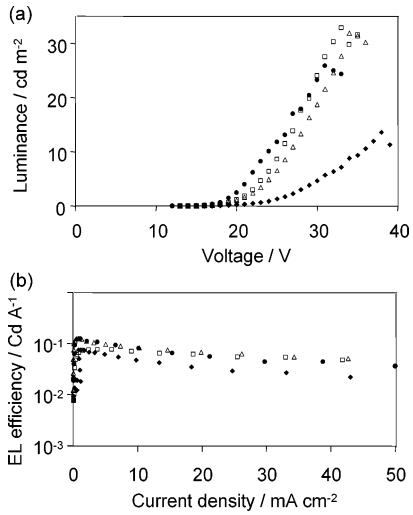

Figure 6. Electro-optical characteristics of electroluminescent devices containing complex **7** at 3 wt % (diamond), 0.7 wt % (circle), 0.07 wt % (triangle), and 0.007 wt % (square): (a) luminance−voltage plot, (b) electroluminescence efficiency plot.

diazole units,[60] have shown that these materials have a higher charge-carrier mobility compared to other oxadiazoles and triarylamines.

Figure 5 shows the emission profiles of **7** doped into an EL device at different doping levels. The lowest doping level shows a blue-green emission from the PVK polymer[11] and Alq_3 layer. However, at doping levels as low as 0.07 wt %, the emission becomes dominated by a feature at 650 nm. This is consistent with emission from the MLCT state of **7**; the electroluminescence differs from the solution phase photoluminescence that originates from a ligand-centered state at 432 nm.

The electro-optical properties of the EL devices are shown in Figure 6. The addition of **7** at higher doping levels impaired the efficiency and light output of the device. These results suggest that the optimal doping level for this dye is close to 0.07 wt %. The devices had luminance−current efficiencies approaching 0.1 Cd A^{-1} at low current densities (Figure 6).

Conclusion

The electronic absorption spectra of these complexes are similar to those observed in other dppz systems. The lowest energy transition in the copper(I) and rhenium(I) complexes is the MLCT, and this appears as a shoulder against the LC band. The spectra of the Ru(II) complexes differs in that they show Ru → bpy transitions at 440 nm. These MLCT transitions involving the ancillary ligands obscure dppz-based transitions.

The electrochemical behavior of these complexes is interesting. The presence of metal moieties significantly stabilizes the first reduction potential, by up to 300 mV. It is also found that the differing substitution, which is at the phz end of the ligand, results in up to 100 mV changes in the reduction potential. These two findings show that the electronic nature of the these substituted dppz ligands differ from that of the unsubstituted dppz. It suggests that, for these complexes, reduction is affecting the structure of the entire ligand.

The fluorescence spectra for these compounds reveal the presence of a number of excited states. The rhenium(I) complexes are dominated by LC emissions, whereas the ruthenium complexes show MLCT emissions; the copper(I) complexes show both types of emission behavior. In addition, the copper(I) complexes show extremely long excited-state lifetimes that appear to be MLCT in origin. Such long-lived copper(I) MLCT excited states normally require substituents about the 3,6 positions to inhibit exciplex formation and excited-state deactivation.[61]

Vibrational spectra of the complexes modeled by DFT display an absolute mean deviation between predicted and observed spectral bands of 6 cm^{-1}. The molecular orbitals provided by DFT calculations point to ligand-based LUMOs that are delocalized across the entire ligand structure. Although these findings contrast with those for unsubstituted dppz in which phen- and phz-based MOs are calculated, they are, nonetheless, consistent with the electrochemical studies.

Electroluminescent devices may be fashioned from these complexes, and in the case of **7**, emission from an MLCT state is observed even at very low doping levels (<0.1% by wt) for the complex. The electroluminescent properties of these complexes will be the subject of further investigation.

Acknowledgment. We thank the MacDiarmid Institute for Advanced Materials and Nanotechnology for providing funding for this work.

Supporting Information Available: Crystallographic data in CIF format. This material is available free of charge via the Internet at http://pubs.acs.org.

IC050179K

(60) Gong, X.; Ng, P. K.; Chan, W. K. *Adv. Mater. (Weinheim, Ger.)* **1998**, *10*, 1337.

(61) Cuttell, D. G.; Kuang, S.-M.; Fanwick, P. E.; McMillin, D. R.; Walton, R. A. *J. Am. Chem. Soc.* **2002**, *124*, 6.